The Bell System Technical Journal
Vol. 53, No. 4, April 1974
Printed in U.S.A.

Slab-Coupled Waveguides

By E. A. J. MARCATILI

(Manuscript received October 16, 1973)

The slab-coupled waveguide, consisting of a dielectric rod lying on a slab that in turn covers a substrate, is a multidielectric waveguide that includes such special cases as the single-material fiber, the rib waveguide, and the strip-loaded film guide. These guides have recently become known as potentially useful either for long-distance optical transmission or for integrated optics.

Simple, closed-form, approximate solutions have been found to describe the following properties of the guide: number of modes, their field configurations and propagation constants, numerical aperture, requirements for single-mode operation, field penetration in the slab, tolerance to curvature of the guide axis, dispersion, and impulse response.

I. INTRODUCTION

Descriptions of three novel diclectric waveguides of wide potential use in long-distance optical transmission and in integrated optics have appeared in tbe literature recently. Tbese guides are tbe single-material fiber[1,2] (Fig. 1) made of low-loss undoped fused silica; tbe rib waveguide[3] (Fig. 2) made of two materials, and the strip-loaded film guide[4,5] (Fig. 3) made of three materials. In all tbese fibers n_3 is air or an inert atmosphere, while in a more general guide it could be another dielectric.

Althougb these guides have different shapes and different distributions of refractive indices, they have essential elements in common that make them close relatives of the same family. A more generic member of this family of waveguides (Fig. 4), from which all the others can be deduced, is a fiber of arbitrary cross section at a distance l from a slab mounted on a substrate. The way in which this guide operates is simpler to understand tban tbe others, and is described below.

The modal spectrum of tbe fiber ($l = \infty$) is shown in Fig. 5(a). In this example, five modes are guided and their axial propagation constants k_z lie between kn_3 and kn_2 where k is the free-space propagation constant $2\pi/\lambda$. Smaller propagation constants tban kn_3 belong to a

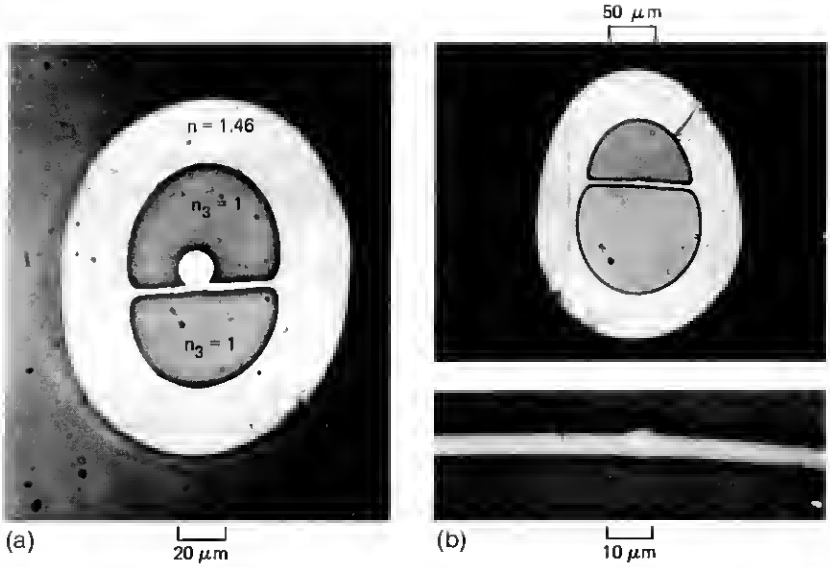

Fig. 1—Photographs of an experimental (a) multimode single-material fiber and (b) single-mode single-material fiber (top), with magnified core region (bottom) ($n > n_3$).

continuum of radiating modes that are unimportant for this discussion. On the other hand, the isolated slab ($l = \infty$) supports modes with q extrema in the y direction. For simplicity we will assume that the field is well confined within the slab. The field components vary sinusoidally along x, y, and z and the respective propagation constants k_x, $k_y = \pi q/t$ and k_z are related by the characteristic equation

$$k_z = \sqrt{k^2 n^2 - k_x^2 - \left(\frac{\pi q}{t}\right)^2}.$$

Since k_z can take any value between zero and infinity, the propagating

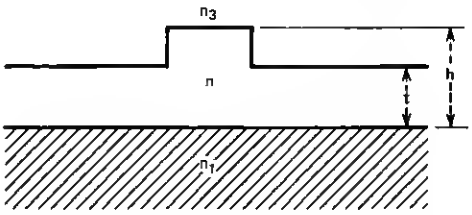

Fig. 2—Rib waveguide ($n > n_1$ and n_3).

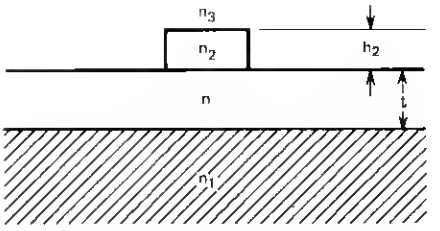

Fig. 3—Optical strip line ($n > n_1$, n_2 and n_3).

modes of the slab with one maximum along y, ($q = 1$) constitute a continuum with axial propagation constants ranging from zero to

$$\sqrt{k^2n^2 - \left(\frac{\pi}{t}\right)^2},$$

as shown in Fig. 5(b). Similarly, propagating slab modes with two extrema along y, ($q = 2$) constitute another continuum witb propagation constants k_z ranging from zero to

$$\sqrt{k^2n^2 - \left(\frac{2\pi}{t}\right)^2},$$

as shown in Fig. 5(c), and so on.

Now let us imagine that, as in Fig. 4, the fiber and tbe slab are separated by a finite distance l which is far enough tbat tbeir respective spectra are only slightly perturbed by the coupling. Modes with the same propagation constant k_z will couple to each other. Therefore,

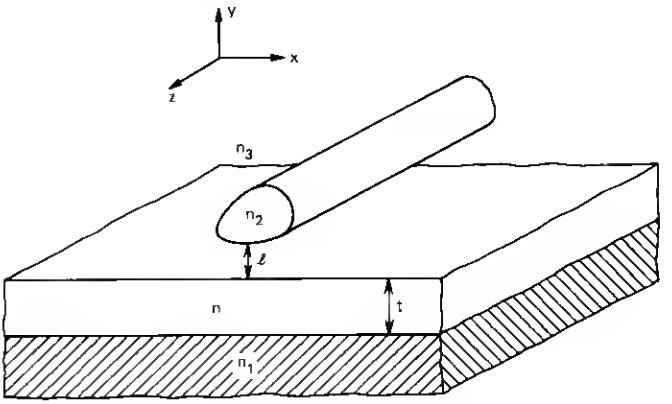

Fig. 4—Slab-loaded waveguide.

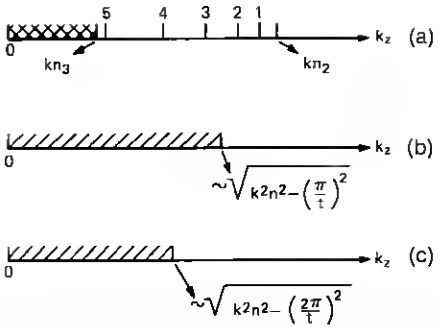

Fig. 5—Modal spectrum in: (a) isolated fiber of Fig. 4; (b) isolated slab of Fig. 4 (only for modes with one half period across t; (c) isolated slab of Fig. 4 (only for modes with two half periods across t).

modes 1 and 2 of the fiher will remain guided without attenuation, tbough tbere is indeed an electromagnetic field in tbe slab that decays exponentially in the x direction (Fig. 4) away from tbe fiber. Mode 3 will couple to tbe slah mode with tbe same k_z of the spectrum in Fig. 5(b); modes 4 and 5 will couple to modes of spectra in Figs. 5(b) and 5(c), etc. The net result is that modes 3, 4, and 5 of the fiher will be attenuated by coupling to slab modes. Tbe smaller tbe distance l between fiber and slab, the tighter the coupling and consequently the bigber tbe attenuation of tbese leaky modes. From Fig. 5 it becomes obvious that by adjusting tbe thickness t of the slab, tbe number of lossless modes can be selected.

The most important point from this discussion is tbat only fiber modes witb axial propagation constants k_z larger tban tbe propagation constant

$$\sqrt{k^2n^2 - \left(\frac{\pi}{t}\right)^2}$$

[Fig. 5(h)] of the slah's fundamental mode are lossless. Therefore, throughout the paper we will he concerned with the coupling between tbe field in tbe core's guide and tbe fundamental mode of tbe slab.

Having identified the three basic elements of this waveguiding structure, a slab, a guide (also referred to as a fiber or strip), and tbe coupling between them, we will use the generic name of slab-coupled guides, fihers, or strips for all the members of this prolific family. Of course, we will reserve tbe names given by tbe original authors to identify individual guides.

Tbe general solution of the slab-coupled guide in Fig. 4 would encompass as particular cases tbose in Figs. 1, 2, and 3. However, only

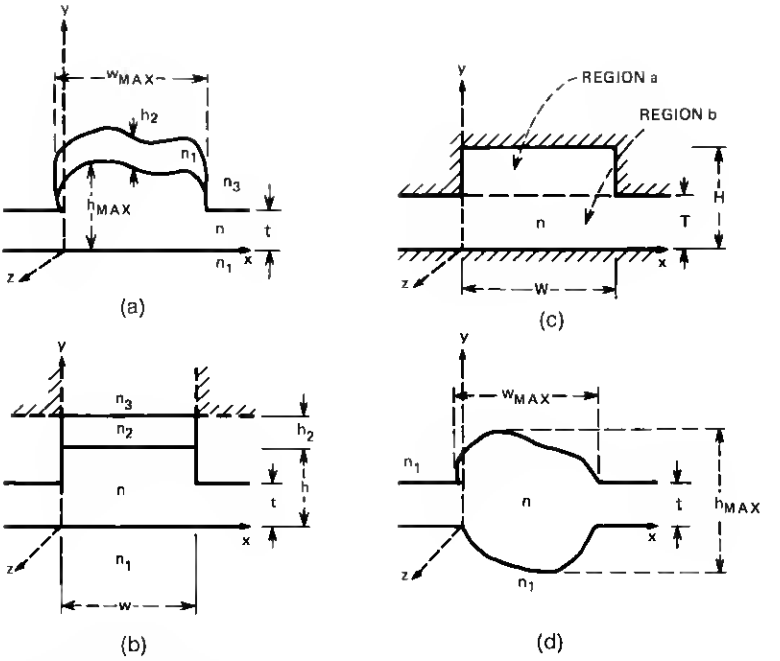

Fig. 6—Slab-coupled waveguide. (a) Original guide. (b) and (c) Equivalent simpler guides. (d) Single-material guide.

two extreme cases seem amenable to closed-form calculations: the case of feeble coupling described in Ref. 6 and the case of strong coupling occurring when the separation between fiber and slab vanishes, and which is the subject of this paper.

In Section II we consider the properties and characteristics of a somewhat generalized slab-coupled guide [Fig. 6(a)]. These are the following:

(*i*) the equivalence to a much simpler guide shown in Fig. 6(c),
(*ii*) the number of guided modes,
(*iii*) their propagation constants and field configurations,
(*iv*) the numerical aperture,
(*v*) the design for single-mode operation,
(*vi*) the field penetration in the slabs,
(*vii*) the tolerance of the guide to the curvature of its axis.

These general results are applied to the multimode and single-mode single-material fibers, rib guides, and strip-loaded guides in Sections III, IV, V, and VI, respectively. Furthermore, dispersion and impulse

response in single-material fibers are considered in Sections III and IV. The simple but burdensome mathematics involved are placed in the appendices to this paper.

II. SOLUTION OF THE SLAB-COUPLED GUIDE

Consider the somewhat generalized slab-coupled guide of Fig. 6(a). It is shown in Appendix B that if

(*i*) most of the electromagnetic energy travels within the region of refractive index n,

(*ii*) the height and the width of the core are almost constants,

(*iii*) there are no turning points within the core ($0 < x < w_{max}$) or, in other words, exponential decay of the field components in the region of refractive index n occurs only in the slabs, and

(*iv*)
$$n > \begin{cases} n_1, \\ n_2, \\ n_3 \end{cases} \tag{1}$$

then the four-dielectric guide with somewhat arbitrarily shaped core in Fig. 6(a) is equivalent to the single-dielectric guide with rectangular core in Fig. 6(c). Surrounding the dielectric of refractive index n, there is a material into which there is no field penetration and the x and y field components of the guided modes vanish at the interface. The dimensions of this equivalent guide are, according to eqs. (83), (84), and (85),

$$T = t(1 + c_t), \tag{2}$$

$$W = w(1 + c_w), \tag{3}$$

$$H = h(1 + c_h), \tag{4}$$

in which the quantities c_t, c_w, and c_h, which are small compared to unity, are from (73), (74), (79), (86) to (89), (100), and (101).

$$c_t = \begin{cases} \dfrac{h}{t}\left(\dfrac{1}{v_1} + \dfrac{1}{v_3}\right) & \text{for modes polarized along } x \\ \dfrac{h}{tn^2}\left(\dfrac{n_1^2}{v_1} + \dfrac{n_3^2}{v_3}\right) & \text{for modes polarized along } y \end{cases} \tag{5}$$

$$c_w = \begin{cases} \dfrac{2h}{wv_3}\dfrac{n_3^2}{n^2} & \text{for modes polarized along } x \\ \dfrac{2h}{wv_3} & \text{for modes polarized along } y \end{cases} \tag{6}$$

$$c_h = \begin{cases} \dfrac{1}{v_1} + \dfrac{1}{v_2} \tanh\left(\dfrac{h_2}{h} v_2 + \tanh^{-1} \dfrac{v_2}{v_3} \right) \\ \qquad\qquad \text{for modes polarized along } x \\ \dfrac{n_1^2}{n^2 v_1} + \dfrac{n_2^2}{n^2 v_2} \tanh\left(\dfrac{h_2}{h} v_2 + \tanh^{-1} \dfrac{n_2^2 v_2}{n_2^2 v_3} \right) \\ \qquad\qquad \text{for modes polarized along } y, \end{cases} \tag{7}$$

where

$$v_{1,2,3} = kh\sqrt{n^2 - n_{1,2,3}^2}\,,^{\dagger} \tag{8}$$

$$h = \sqrt{\frac{h_{\max}}{w_{\max}}}\, s, \tag{9}$$

$$w = \sqrt{\frac{w_{\max}}{h_{\max}}}\, s, \tag{10}$$

and $h_{\max}$ and $w_{\max}$ are the maximum height and width of the portion of the core with refractive index n in Fig. 6(a) and s is its cross-sectional area. All these expressions are valid for

$$v > \begin{cases} \dfrac{\pi}{2} - \tan^{-1} \sqrt{\dfrac{n^2 - n_1^2}{n_1^2 - n_3^2}} & \text{for modes polarized along } x \\ \dfrac{\pi}{2} - \tan^{-1} \dfrac{n_3^2}{n^2} \sqrt{\dfrac{n^2 - n_1^2}{n_1^2 - n_3^2}} & \text{for modes polarized along } y, \end{cases} \tag{11}$$

where

$$v = kt\sqrt{n^2 - n_1^2}. \tag{12}$$

Four parameters, then, n, T, W, and H, determine the guide in Fig. 6(c) and we proceed to characterize its transmission properties.

The guided modes are hybrid; however, the longitudinal field components (along z) are small compared to the transverse ones; therefore, the modes are almost transverse electromagnetic (TEM). Within the core, these transverse field components vary sinusoidally along x and y. Within the slab, the field components also vary sinusoidally along y but decay exponentially away from the core. All these components vanish at the edge of the guide.

There are two families of modes, E_{pq}^{y} and E_{pq}^{z}. The first family, Fig. 7(a), is mostly polarized along y, and the main transverse field components are E_y and H_x. Within the core, a mode has p field extrema (approximately p half periods) along x and q field extrema along y.

[†] Throughout this paper numbers or letters separated by commas must be considered one at a time.

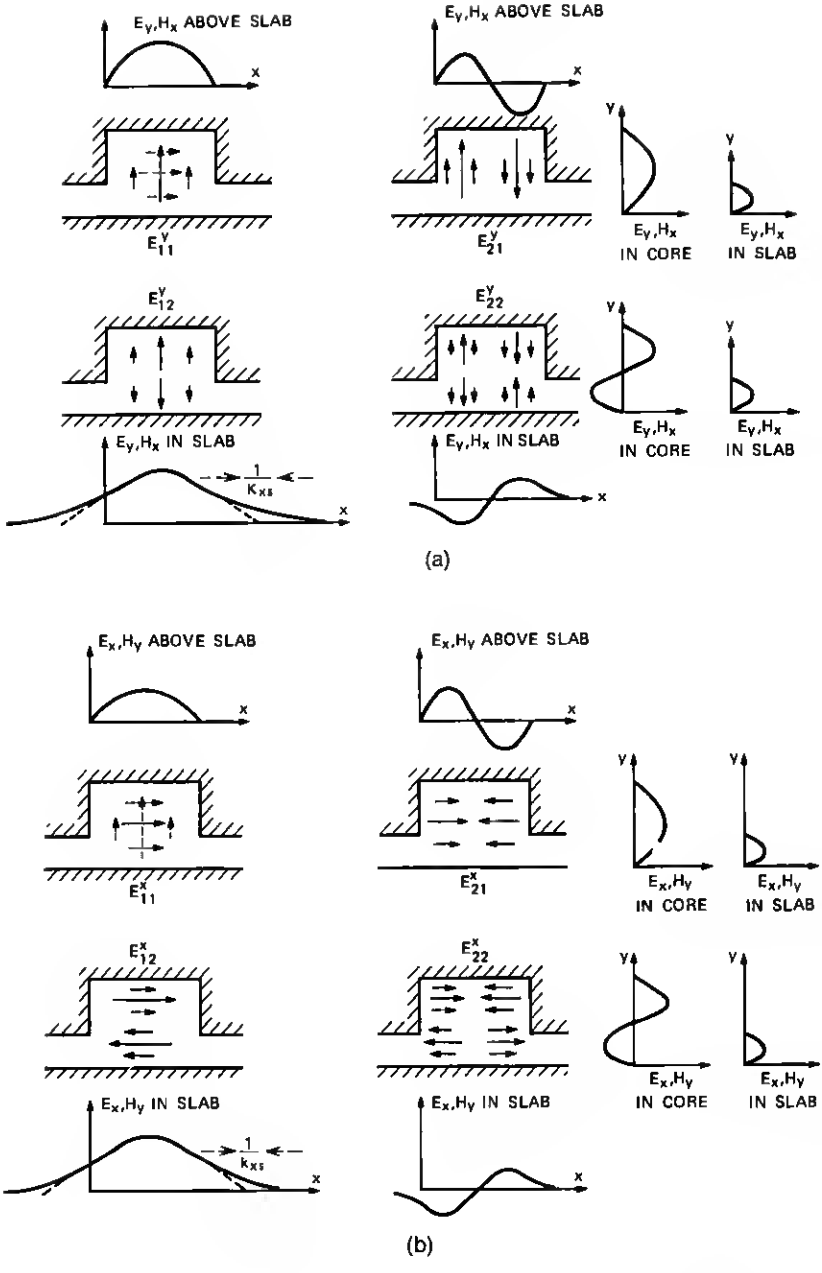

Fig. 7—Two families of modes. (a) E_{pq}^y modes and (b) E_{pq}^x modes.

The second family of modes, Fig. 7(b), is mostly polarized along x and the main transverse components are E_x and H_y.

For both families, the axial propagation constant k_z and the field penetration in the slabs d_{pq}, that is the distance over which the field components decay in the slabs by $1/e$, are according to (98) and (99),

$$k_z = \sqrt{k^2 n^2 - \left[\frac{\pi p}{W(1 + c_q)}\right]^2 - \left(\frac{\pi q}{H}\right)^2} \tag{13}$$

$$k_{xs} = \frac{1}{d_{pq}} = \frac{\pi}{T}\sqrt{1 - \left[\frac{pT}{W(1 + c_q)}\right]^2 - \left(\frac{qT}{H}\right)^2}, \tag{14}$$

where c_q taken from (97) is

$$c_q = \frac{2}{\pi}\frac{T^2}{WH}\frac{1}{\sqrt{1 - \left(\frac{qT}{H}\right)^2}}. \tag{15}$$

The highest-order modes, which we will designate with indices $p = P$ and $q = Q$, are those for which the penetration depth d_{PQ} is infinite. For them, eqs. (13) and (14) are reduced to

$$\sqrt{n^2 - \frac{k_{z\min}^2}{k^2}} = \frac{\lambda}{2T} = \text{N.A.} \tag{16}$$

and

$$\frac{PT}{W} - \sqrt{1 - \left(\frac{QT}{H}\right)^2} = \frac{2}{\pi}\frac{T^2}{WH}. \tag{17}$$

While for ordinary fibers, the numerical aperture (N.A.) $\sqrt{n^2 - n_e^2}$ is an exclusive function of the refractive indices of the core n, and the cladding n_e, the N.A. of a slab-coupled guide defined in (16) is mostly a function of the wavelength and the slab thickness. The longer the wavelength and the thinner the slab, the larger the numerical aperture. This statement is true provided that the inequality (11) is satisfied.

Naturally, an equivalent cladding refractive index

$$n_e = \sqrt{n^2 - \left(\frac{\lambda}{2T}\right)^2} \tag{18}$$

is derived by equating $k_{z\min}/k$ to n_e.

The easiest property to observe in slab-coupled guides is, probably, the number of spots of the highest order mode guided. That number is the product of P and Q which are related to each other by eq. (17).

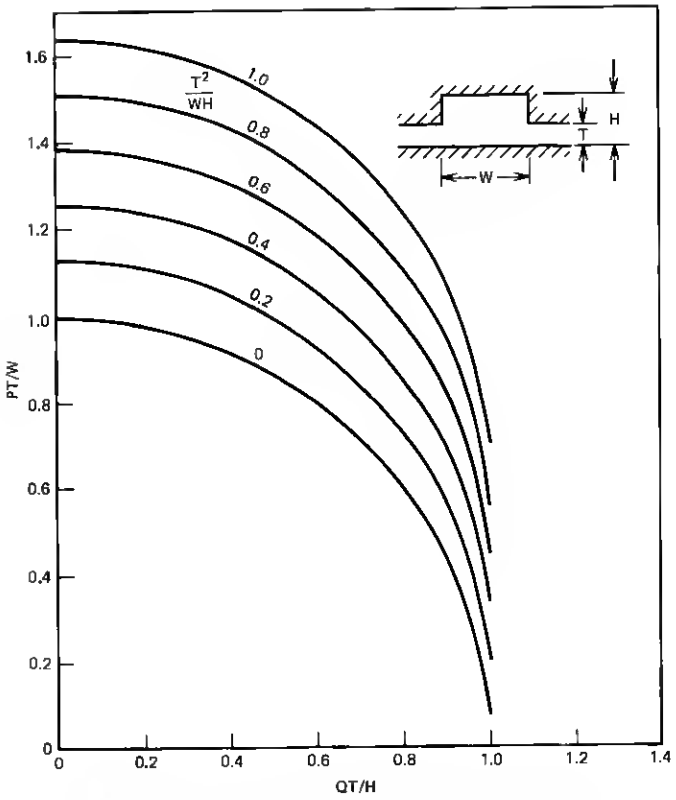

Fig. 8—Waveguide dimensions for $E^{z,y}_{PQ}$ mode at cutoff.

A plot using PT/W and QT/H as coordinates and T^2/WH as the parameter is shown in Fig. 8. Given T/W and T/H, the parameter T^2/WH, which selects one of these curves in Fig. 8, is also known. For the ordinate T/W corresponding to $P = 1$, the abscissa $Q_{\max}\ T/H$ is determined and from it the maximum number of half periods $Q_{\max}$ of the modes $E^{z,y}_{1Q_{\max}}$ in the y direction. Similarly for the abscissa T/H corresponding to $Q = 1$, the ordinate $P_{\max}\ T/W$ yields the maximum number of half periods $P_{\max}$ of the modes $E^{z,y}_{P_{\max}1}$ in the x direction.

Example: For $T/H = 0.5$ and $T/W = 0.1$, the values $P_{\max} = 8$ and $Q_{\max} = 1$ (rounded off to the immediate lower integer) are obtained.

The explicit values of $P_{\max}$ and $Q_{\max}$ derived from (17) are

$$P_{\max} = \frac{W}{T}\left[\sqrt{1 - \left(\frac{T}{H}\right)^2} + \frac{2}{\pi}\frac{T^2}{WH}\right] \tag{19}$$

and

$$Q_{\max} = \frac{H}{T}\left[1 - \left(\frac{T}{W}\right)^2\left(1 - \frac{2T}{\pi H}\right)^2\right]^{\frac{1}{2}}. \tag{20}$$

From this last equation,

$$T < \frac{H}{Q_{\max}}. \tag{21}$$

Consequently, for any guided mode the slab thickness T is always smaller than the half period of the mode in the core along y. This justifies one of the assumptions in Appendix B.

The guide is largely overmoded if

$$\frac{T}{W} \ll 1 \tag{22}$$

and

$$\frac{T}{H} \ll 1; \tag{23}$$

then, the number of modes for each polarization deduced from (19) and (20) results in

$$N = \frac{\pi}{4}\frac{WH}{T^2}. \tag{24}$$

Unlike ordinary fibers, the number of modes of a slab-coupled guide is mostly determined by its geometry.

To dimension the slab-coupled guide for single-mode operation, eq. (17) has been plotted in Fig. 9 using T/H and T/W as variables plus two sets of parameters $P = 1$, $Q = 2$ and $P = 2$, $Q = 1$. The coordinates of the first line give the dimensions of a guide with the E^x_{12} and E^y_{12} modes at cutoff while those in the second line yield the guide dimension with the E^x_{21} and E^y_{21} modes at cutoff. The solid portions of both curves determine the smallest possible ratios T/W and T/H compatible with single-mode guidance. The discrete numbers on the curves indicate the ratio H/W. For a square core ($H = W$) we deduce from the figure that $T/W \simeq T/H \simeq 0.5$.

For the fundamental mode, the field penetration in the slabs, d_{11}, is obtained from (14), making $p = q = 1$. With rearranged terms, eq. (14) reads

$$\frac{W}{T} = \frac{1}{\sqrt{1 - \left(\frac{T}{H}\right)^2 - \left(\frac{T}{\pi d_{11}}\right)^2}} - \frac{2T}{\pi H}\frac{1}{\sqrt{1 - \left(\frac{T}{H}\right)^2}} \tag{25}$$

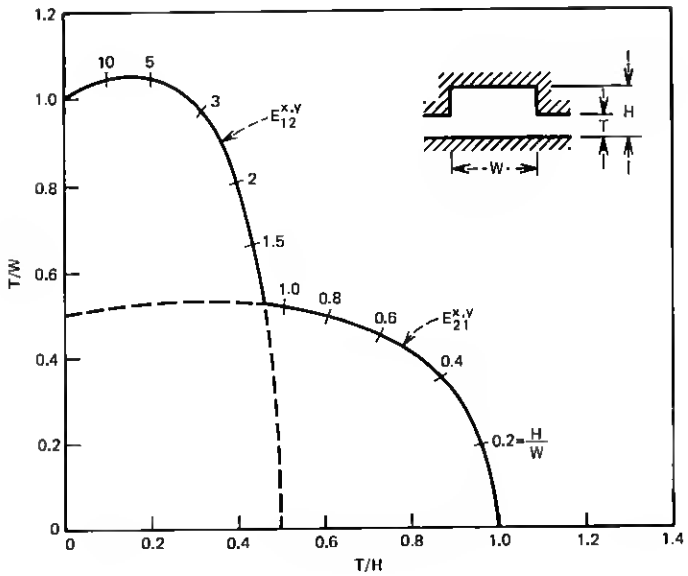

Fig. 9—Waveguide dimensions for $E_{12}^{x,y}$ and $E_{21}^{x,y}$ modes at cutoff.

and it is plotted as solid lines in Fig. 10 using T/H and T/W as coordinates and T/d_{11} as the parameter.

In the same figure, the dotted line is a reproduction of the curve of Fig. 9 corresponding to the cutoff condition of the $E_{12}^{x,y}$ and $E_{21}^{y,x}$ modes. The intersection of this curve with the others yields, then, the field penetration of the fundamental modes in guides designed to be at cutoff for the next higher order modes.

The region between the solid curve with parameter $T/d_{11} = 0$ (infinite field penetration in the slab) and the dotted curve delimits the possible choices of T/H and T/W for single-mode waveguides. The region within the dotted curve corresponds to multimode waveguides.

Let us consider now the attenuation of the fundamental mode due to radiation induced by the curvature of the guide's axis. If the guide axis is bent in the plane of the slab along a constant radius of curvature R, the attenuation of the fundamental mode in a 90° bend[7,8] is proportional to

$$R \exp\left[- \frac{1}{6\pi^2 n^2} \frac{\lambda^2 R}{d_{11}^3} \right] \tag{26}$$

and it is negligibly small if[7]

$$R \geqq 24 \left(\frac{\pi n}{\lambda} \right)^2 d_{11}^3. \tag{27}$$

The tolerable radius of curvature decreases rapidly with d_{11}.

Shorter radii of curvature can be negotiated in the plane perpendicular to the slabs if, as it happens in general, the field penetrations from the slabs into the media of indices n_1 and n_3 are smaller than d_{11}.

We can reuse Fig. 10 by substituting the parameter T/d_{11} with its equivalent

$$6.2 \left(\frac{n^2 T^3}{R\lambda^2} \right)^{\frac{1}{3}}$$

deduced from the equality in (27). For single-mode waveguides, the shortest d_{11} and consequently the shortest tolerable radius of curvature is achieved for $T/H \simeq T/W \simeq 0.5$.

The pertinent calculations for curvature-induced losses in multimode slab-coupled guides are carried on in Section III, where multimode single-material fibers are considered.

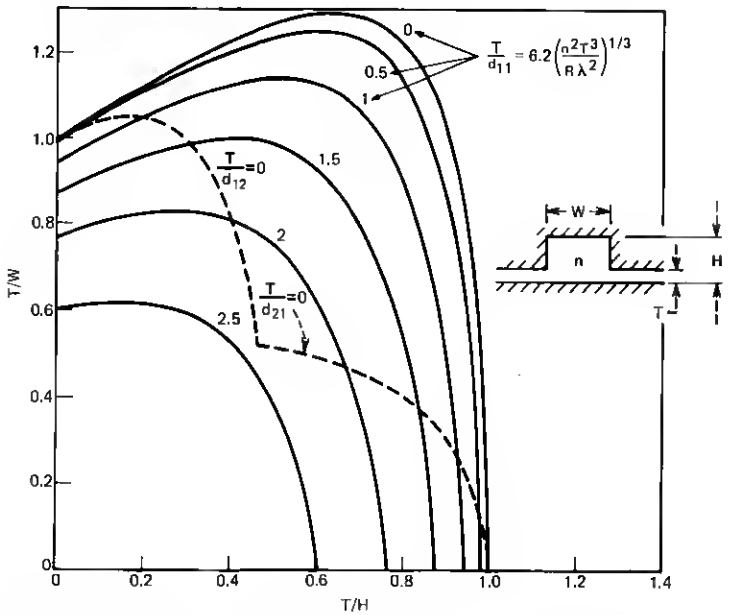

Fig. 10—Field penetration in slab d_{11} and tolerable radius of curvature R for fundamental mode.

III. MULTIMODE SINGLE-MATERIAL FIBERS

Single-material fibers supporting any number of modes, Fig. 1(a), are characterized by

$$n_1 = n_2 = n_3 = 1. \tag{28}$$

Under these circumstances, the location of the slab with respect to the core in Fig. 6(a) is not taken into account by the theory presented in this paper and, consequently, a more general cross section of single-material fibers is shown in Fig. 6(d). Figure 6(c) is still its equivalent (Appendix B).

Multimode single-material fibers satisfy not only (28) but also the following inequalities

$$\left.\begin{matrix} \frac{h}{t} \\ \frac{w}{t} \\ \frac{2t}{\lambda} \end{matrix}\right\} \gg 1. \tag{29}$$

Therefore, parameters (2), (3), and (4) defining the guide are substantially simplified

$$T = t \tag{30}$$

$$W = w \tag{31}$$

$$H = h \tag{32}$$

and are valid for all polarizations.

According to (30), (31), and (32), the electromagnetic field is well confined within the guide. Using these values, the numerical aperture (16), the equivalent external refractive index (18), the number of modes for both polarizations (24), and the propagation constant for each mode (13) are

$$\text{N.A.} = \frac{\lambda}{2t} \ll 1, \tag{33}$$

$$n_e = \sqrt{n^2 - \left(\frac{\lambda}{2t}\right)^2} \cong n\left[1 - \frac{1}{8}\left(\frac{\lambda}{nt}\right)^2\right], \tag{34}$$

$$N = \frac{\pi}{2}\frac{S}{t^2}, \tag{35}$$

and

$$k_z = \sqrt{k^2 n^2 - \left(\frac{\pi p}{w}\right)^2 - \left(\frac{\pi q}{h}\right)^2}, \tag{36}$$

where S is the core cross-sectional area.

Unlike ordinary guides the number of modes N is independent of the free-space wavelength λ. In other words, by keeping λ fixed, the scale of the guide's cross section could be changed without varying the number of guided modes! How is it possible? The following is a plausible argument. For a given wavelength, if S is increased the number of guided modes in the core should increase, but simultaneously the number of modes that can escape through the enlarged slabs is also increased. The fact that both increases compensate for each other can only by justified with the mathematics.

Let us turn now to modal dispersion. Calling L the length of the guide and c the speed of light in free space, the group delay spread between any mode with propagation constant k_z and the fundamental one[9] (which has a propagation constant very close to that of a plane wave in a medium of refractive index n) is

$$\tau = \frac{L}{c}\frac{d}{dk}(k_z - kn). \tag{37}$$

With the help of (36)

$$\tau = \frac{Ln}{c}\left(\frac{kn}{k_z} - 1\right). \tag{38}$$

The maximum time spread occurs for the highest order mode which has the smallest k_z value, kn_e. Then, using (34) for the value of n_e,

$$\tau_{\max} = \frac{L}{c} n \left(\frac{n}{n_e} - 1\right) = \frac{L}{8nc}\left(\frac{\lambda}{t}\right)^2. \tag{39}$$

The impulse response is similar to that of clad fibers. A short impulse feeding equally all of the guided modes arrives at the other end as many impulses unequally displaced in time.[10] However, the power density of the arriving pulse is uniform over the time interval $\tau_{\max}$ given in (39) and zero elsewhere. This impulse response width being inversely proportional to the square of the slab thickness can be shortened by increasing t.

Since there is more familiarity with clad fibers than with single-material fibers, it is of interest to make a comparison between them,

assuming both guide the same number of modes N, and have the same modal dispersion spread τ_{max}. For a clad fiber of radius a and core and cladding refractive indices n and $n(1 - \Delta)$, those values are[11,9]

$$N = \left(\frac{2\pi an}{\lambda}\right)^2 \Delta \tag{40}$$

and

$$\tau_{max} = \frac{L}{C} n\Delta. \tag{41}$$

These two equations together with (35) and (39) are plotted in Fig. 11. The group of curves on the lower part corresponds to single-material guides, and those on the upper part correspond to the equivalent clad fiber. Dotted lines are for the modal dispersion spread and solid lines for the number of modes. The parameters are either the core diameter of the clad fiber or the square root of the core cross section of the single-material fiber normalized in both cases to the free-space wavelength.

Example: For a dispersion spread τ of 26 ns/km and $N/n = 100$, the single-material fiber dimensions are $t\sqrt{n}/\lambda = 4$ and $\sqrt{S}/\lambda = 31.6$, while those of the equivalent clad fiber are $n\Delta = 0.008$ and $2a/\lambda = 36$.

If the multimode single-material fiber is bent, all the modes become somewhat lossy; however, as in ordinary clad fibers the radiation loss is significant only for those modes whose plane wave components exceed the critical angle. Unlike clad guides, though, a bend in the plane of the slabs produces higher losses than a similar bend in the perpendicular plane. This is due to the fact that, for a given mode, the field penetration in the slabs is far larger than in the material of index n_1.

The single-material fiber bent in the plane of the slabs on a radius of curvature R has a numerical aperture N.A.′ and guides a number of modes[12] N', both of them smaller than the N.A. (33) and the number of modes (35) of the straight guide. As a matter of fact,

$$\text{N.A.}' = \frac{\lambda}{2t}\left[1 - \frac{w}{R}\left(\frac{2nt}{\lambda}\right)^2\right] \tag{42}$$

and

$$N' = \frac{\pi}{2}\frac{S}{t^2}\left[1 - 2\frac{w}{R}\left(\frac{2nt}{\lambda}\right)^2\right]. \tag{43}$$

Only half of the modes remain guided if

$$R_{\frac{1}{2}} = w\left(\frac{4nt}{\lambda}\right)^2. \tag{44}$$

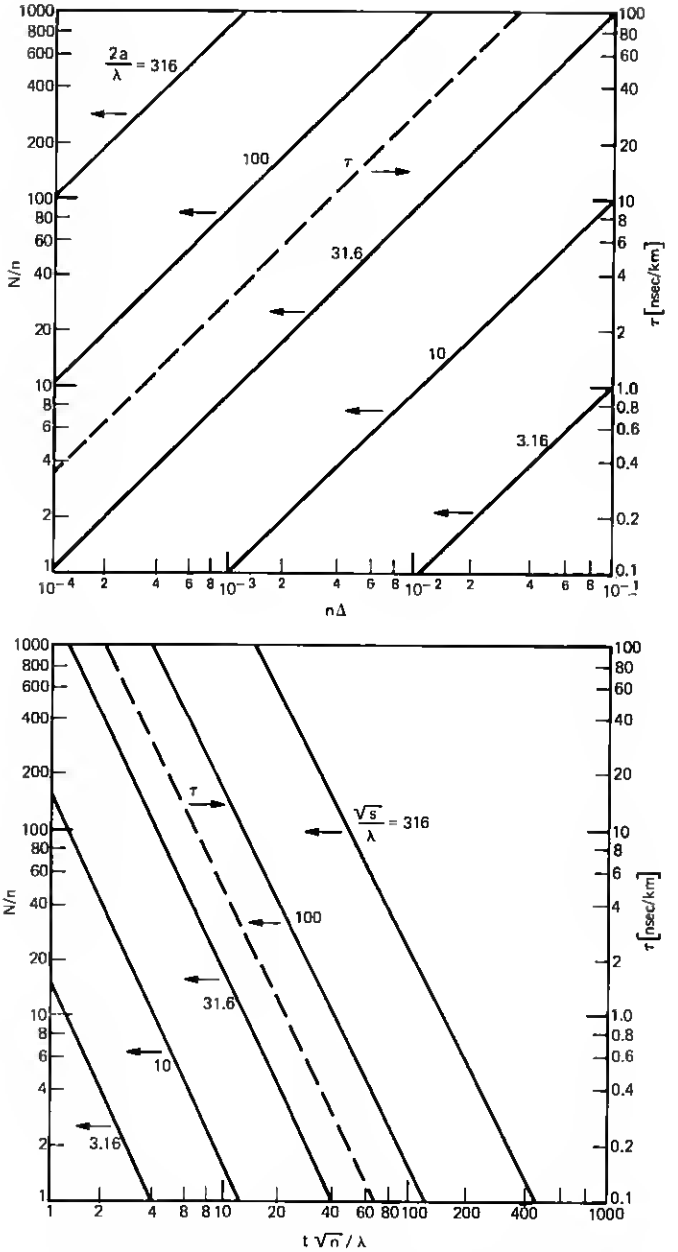

Fig. 11—Multimode single-material fiber and its equivalent clad fiber.

Example: For $n = 1.5$, $t/\lambda = 2$ and $w = 50\,\mu$, from the previous formula follows

$$R_{\frac{1}{2}} = 7.2 \text{ mm},$$

a small radius indeed.

IV. SINGLE-MODE SINGLE-MATERIAL FIBERS

In single-mode single-material fibers, Fig. 1(h), of interest for optical communication, all of the dimensions are large compared to the wavelength of operation. Therefore, eqs. (28) through (32) are valid and all formulas and figures of Section II related to the fundamental mode in slab-coupled guides are applicable just by changing T, H, and W into t, h, and w, respectively.

The dimensional requirements for single-mode operation with the next higher order at cutoff are determined by the solid line in Fig. 9. For example, it may be that for splicing purposes it is desirable to have a core of square cross section; then, from that figure,

$$h = w = 2t. \tag{45}$$

As in the multimode case, these dimensional requirements are independent of the wavelength and, consequently, the cross section of the guide can be scaled to satisfy other demands, such as relief of splicing tolerances, simplicity of fabrication, etc.

The propagation constant of the fundamental mode for both polarizations (13), the field penetration in the slabs (14), and the tolerable radius of curvature (27) are

$$k_z = \sqrt{k^2 n^2 - \pi^2 \left[\frac{1}{h^2} + \frac{1}{w^2(1 + c_1)^2} \right]}, \tag{46}$$

$$\frac{1}{d_{11}} = \pi \sqrt{\frac{1}{t^2} - \frac{1}{h^2} - \frac{1}{w^2(1 + c_1)^2}}, \tag{47}$$

and

$$R = \frac{24}{\pi} \left(\frac{n}{\lambda} \right)^2 \frac{t^3}{\left[1 - \frac{t^2}{h^2} - \frac{t^2}{w^2(1 + c_1)^2} \right]^{\frac{1}{2}}}, \tag{48}$$

where

$$c_1 = \frac{2}{\pi} \frac{t^2}{wh} \frac{1}{\sqrt{1 - \left(\frac{t}{h} \right)^2}}. \tag{49}$$

Normalized values of d_{11} and R can be found as parameters in Fig. 10

Table I

t (μm) \ t/h	0.33	0.5	0.9	0.33
t (μm) \ t/w	0.53	0.51	0.33	0.1
2	0.23 mm	0.32 mm	2.6 mm	74 mm
5	2.1	4.9	40.0	115
10	17.0	40.0	330.0	925
Mode at Cutoff	$E_{21}^{z,y}$	$E_{21}^{z,y}$	$E_{21}^{z,y}$	$E_{13}^{z,y}$

for different values of t/h and t/w. Points on the dotted curve belong to single-mode guides with either the $E_{12}^{z,y}$ or $E_{21}^{z,y}$ modes at cutoff.

Continuing with the practical example above in which $h = w = 2t$, we obtain either from (47) or from Fig. 10

$$d_{11} = 0.42t. \tag{50}$$

With the help of (48) or Fig. 10, one can calculate a table of tolerable radii of curvature (Table I) for the fundamental mode in a guide with either the $E_{12}^{z,y}$ or $E_{21}^{z,y}$ modes at cutoff and assuming $n = 1.5$ and $\lambda = 1$ μm.

Shorter radii of curvature are achieved for smaller t and t/h ratios if the guide is designed for the $E_{21}^{z,y}$ modes at cutoff (see Table I, first three columns). As seen from the last column, guides designed for $E_{12}^{z,y}$ modes at cutoff have longer tolerable radii of curvature. The guidance is not as tight and consequently less desirable.

Let us turn to dispersion. Knowing k_z (46) it is possible to calculate the dispersion $(L/c)(\partial k_z/\partial k)$ in a guide of length L. However, a more interesting result is the guide response to a Gaussian input pulse of $1/e$ width T_0. Following standard techniques to calculate responses through linear devices, one finds the output to be close to another Gaussian whose $1/e$ width is

$$T = T_0 \sqrt{1 + \left[\frac{2L}{c^2 T_0^2} \frac{\partial^2 k_z}{\partial k^2} \right]_{k=k_0}^2}. \tag{51}$$

The second derivative is to be calculated at the wave number k_0 of the carrier and c is the free-space speed of light.

For a given length of fiber L', the input pulse width T_0 that minimizes the output pulse width ($T' = \sqrt{2}T_0$) is related to L' by

$$L' = \frac{c^2 T_0^2}{2} \frac{1}{\left(\dfrac{\partial^2 k_z}{\partial k^2} \right)_{k=k_0}}. \tag{52}$$

Assuming (46) to be applicable and $c_1 \ll 1$,

$$L' = 4\pi n \frac{c^2 T_0^2}{\lambda^3} \frac{h^2 w^2}{h^2 + w^2}. \tag{53}$$

Example: For

$$n = 1.5,$$
$$T_o = 10 \text{ ps},$$
$$h = w = 20\,\mu m,$$

and

$$\lambda = 1\,\mu m,$$

then,

$$L' = 34 \text{ km}.$$

As expected, the waveguide dispersion of the fundamental mode in a single-material fiber is very small and material dispersion may be more significant.[10]

V. RIB WAVEGUIDES

These slab-coupled guides, Figs. 2 and 6(b), are characterized by

$$n_2 = n_3 = 1, \tag{54}$$

$$\frac{n - n_1}{n} \ll 1, \tag{55}$$

and h slightly larger than t. Substituting (54) and (55) in (2), (3), and (4), the dimensions of the equivalent guides in Fig. 6(c) are

$$T = \begin{cases} t\left(1 + \dfrac{1}{v}\right) & \text{for } E^x_{pq} \text{ modes} \\ t\left(1 + \dfrac{n_1^2}{n^2 v}\right) & \text{for } E^y_{pq} \text{ modes,} \end{cases} \tag{56}$$

$$W = w \qquad \text{for } E^{xy}_{pq} \text{ modes,} \tag{57}$$

and

$$H = \begin{cases} h\left(1 + \dfrac{t}{hv}\right) & \text{for } E^x_{pq} \text{ modes} \\ h\left(1 + \dfrac{n_1^2 t}{n^2 hv}\right) & \text{for } E^y_{pq} \text{ modes,} \end{cases} \tag{58}$$

where

$$v = kt\sqrt{n^2 - n_1^2}. \tag{59}$$

Simplified by (54) and (55), eq. (11) says that expressions (56) and (58) are valid provided

$$v > \begin{cases} \dfrac{\pi}{2} - \sqrt{\dfrac{n^2 - n_1^2}{n_1^2 - 1}} & \text{for } E_{pq}^{x} \text{ modes} \\ \dfrac{\pi}{2} - \dfrac{1}{n^2}\sqrt{\dfrac{n^2 - n_1^2}{n_1^2 - 1}} & \text{for } E_{pq}^{y} \text{ modes.} \end{cases} \tag{60}$$

Using the values T, W, and H given by (56), (57) and (58) in previous equations and figures, the following results can be ascertained:

(*i*) Propagation constants of different modes and polarizations (13),

(*ii*) Maximum number of half periods $P_{\max}$ and $Q_{\max}$, in the highest order modes $E_{1Q_{\max}}^{x,y}$ and $E_{P_{\max}1}^{x,y}$ [(19) and (20) or Fig. 8],

(*iii*) Dimensions of the guide for single-mode operation with the next higher order mode at cutoff [(17) or Fig. 9],

(*iv*) Field penetration in slabs d_{11} for the fundamental modes [(25) or Fig. 10],

(*v*) Tolerable radii of curvature in the plane of the slabs for the fundamental mode [(27) or Fig. 10].

VI. STRIP-COUPLED GUIDE

This guide, Figs. 3 and 6(b), is characterized by

$$n_3 = 1, \tag{61}$$

$$\frac{n - n_1}{n} \ll 1, \tag{62}$$

$$\frac{n - n_2}{n} \ll 1, \tag{63}$$

and

$$h = t. \tag{64}$$

Substituting (61) through (64) in (2), (3), and (4), the dimensions of the equivalent guide in Fig. 6(c) are

$$T = \begin{cases} t\left(1 + \dfrac{1}{v_1}\right) & \text{for } E_{pq}^{x} \text{ modes} \\ t\left(1 + \dfrac{n_1^2}{n^2 v_1}\right) & \text{for } E_{pq}^{y} \text{ modes,} \end{cases} \tag{65}$$

$$W = w \qquad \text{for } E_{pq}^{x,y} \text{ modes,} \tag{66}$$

$$H = \begin{cases} t\left(1 + \dfrac{1}{v_1} + \dfrac{1}{v_2}\tanh\dfrac{h_2 v_2}{t}\right) & \text{for } E_{pq}^{x} \text{ modes} \\ t\left(1 + \dfrac{n_1^2}{n^2 v_1} + \dfrac{n_2^2}{n^2 v_2}\tanh\dfrac{h_2 v_2}{t}\right) & \text{for } E_{pq}^{y} \text{ modes,} \end{cases} \tag{67}$$

where

$$v_{1,2} = kt\sqrt{n^2 - n_{1,2}^2}. \tag{68}$$

These expressions are valid only if, according to (11) simplified by (61) through (64),

$$v_1 > \begin{cases} \dfrac{\pi}{2} - \sqrt{\dfrac{n^2 - n_1^2}{n_1^2 - 1}} & \text{for } E_{pq}^x \text{ modes} \\ \dfrac{\pi}{2} - \dfrac{1}{n^2}\sqrt{\dfrac{n^2 - n_1^2}{n_1^2 - 1}} & \text{for } E_{pq}^y \text{ modes.} \end{cases} \tag{69}$$

It should he noticed that H cannot he made much larger than T just by increasing h_2 because the field decays almost exponentially along y in the material of index n_2, Fig. 6(h). As a matter of fact, the maximum value H is

$$h_{\max} = \begin{cases} t\left(1 + \dfrac{1}{v_1} + \dfrac{1}{v_2}\right) & \text{for } E_{pq}^x \text{ modes} \\ t\left(1 + \dfrac{n_1^2}{n^2 v_1} + \dfrac{n_2^2}{n^2 v^2}\right) & \text{for } E_{pq}^y \text{ modes.} \end{cases} \tag{70}$$

As in the rib waveguide the values of T, W, and H in (65), (66), and (67) can be entered in previous formulas and figures to find propagation constants of modes polarized along either x or y (13); number of guided modes [(19) and (20) or Fig. 8]; dimensions of guide for fundamental mode operation with the next higher order at cutoff [(17) or Fig. 9]; field penetration in slahs for the fundamental modes [(25) or Fig. 10]; tolerable radius of curvature for the fundamental mode [(27) or Fig. 10].

ACKNOWLEDGMENT

The author is grateful to Mmes. W. Mammel and D. Vitello for their computational contrihutions and to Messrs. S. E. Miller, J. Arnaud, and D. Marcuse for stimulating and demanding discussions.

APPENDIX A

Approximate solution of the slab

Consider the two-layer slab in Fig. 12(a). Propagating along z, the field components are independent of x and the characteristic equa-

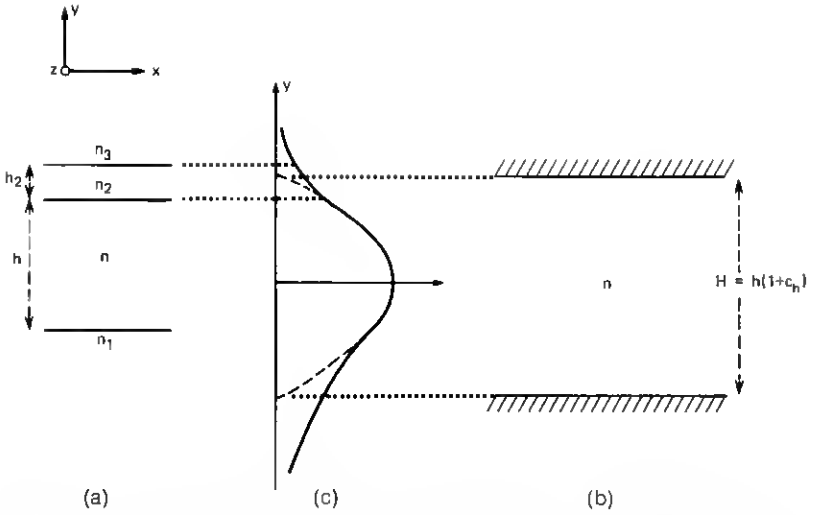

Fig. 12—(a) Two-layered slab. (b) Equivalent slab. (c) Field distributions (E_x and H_y or E_y and H_x) in original slab (solid line) and in equivalent slab (dotted line).

tion[13] is

$$\pi q = \psi + \tan^{-1} \frac{K_1 \psi}{\sqrt{v_1^2 - \psi^2}}$$

$$+ tan^{-1} \left\{ \frac{K_2 \psi}{\sqrt{v_2^2 - \psi^2}} \tanh \left[\frac{h_2}{h} \sqrt{v_2^2 - \psi^2} + \tanh^{-1} \frac{K_3}{K_2} \sqrt{\frac{v_2^2 - \psi^2}{v_3^2 - \psi^2}} \right] \right\}, \quad (71)$$

where

$$\psi = k_y h \quad (72)$$

is the electrical height of the slab of index n; q is the number of field extrema within the slab;

$$K_{1,2,3} = \begin{cases} \dfrac{n_{1,2,3}^2}{n^2} & \text{for polarization along } y \\ 1 & \text{for polarization along } z, \end{cases} \quad (73)$$

$$v_{1,2,3} = kh\sqrt{n^2 - n_{1,2,3}^2}. \quad (74)$$

Assuming

$$n > \begin{cases} n_1 \\ n_2, \\ n_3 \end{cases} \quad (75)$$

the field components vary sinusoidally along y in the medium of index n and exponentially in the others.

Real solutions of (71), which correspond to guided modes, exist for values of v_1 larger than

$$v_{\min} = \pi\left(q - \frac{1}{2}\right) - \tan^{-1}\left\{K_2\sqrt{\frac{n^2 - n_1^2}{n_1^2 - n_2^2}} \cdot \tanh\left[\frac{h_2}{h}\sqrt{v_2^2 - v_1^2} + \tanh^{-1}\frac{K_3}{K_2}\sqrt{\frac{n_1^2 - n_2^2}{n_1^2 - n_3^2}}\right]\right\}. \quad (76)$$

The simple asymptotic solution of (71) for

$$v_1 \gg v_{\min} \quad (77)$$

is

$$\psi = \frac{\pi q}{1 + c_h}, \quad (78)$$

where

$$c_h = \frac{K_1}{v_1} + \frac{K_2}{v_2}\tanh\left(\frac{h_2}{h}v_2 + \tanh^{-1}\frac{K_3}{K_2}\frac{v_2}{v_3}\right). \quad (79)$$

The asymptotic solution (78) and the exact solution have been plotted in Figs. 13(a), (b), and (c) for several cases of interest.

Since the percentile errors are small, even close to the cutoff values of v_1, expression (78) will be used throughout the paper.

Now we proceed to find a much simpler slab [Fig. 12(h)] that is equivalent to that of Fig. 12(a) in the sense that hoth have the same propagation constants

$$k_y = \frac{\pi q}{h(1 + c_h)} \quad (80)$$

and

$$k_x = \sqrt{k^2 n^2 - k_y^2}. \quad (81)$$

That is indeed the case if the slab in Fig. 12(h) has refractive index n, height

$$H = h(1 + c_h), \quad (82)$$

and is surrounded hy a hypothetical dielectric* such that all the transverse field components (components along x and y) vanish at the interfaces. This dielectric plays only the role of confining the electromagnetic field within the slah.

---

*This hypothetical dielectric has infinite conductivity if $E_x \neq 0$ or infinite permeability if $H_x \neq 0$.

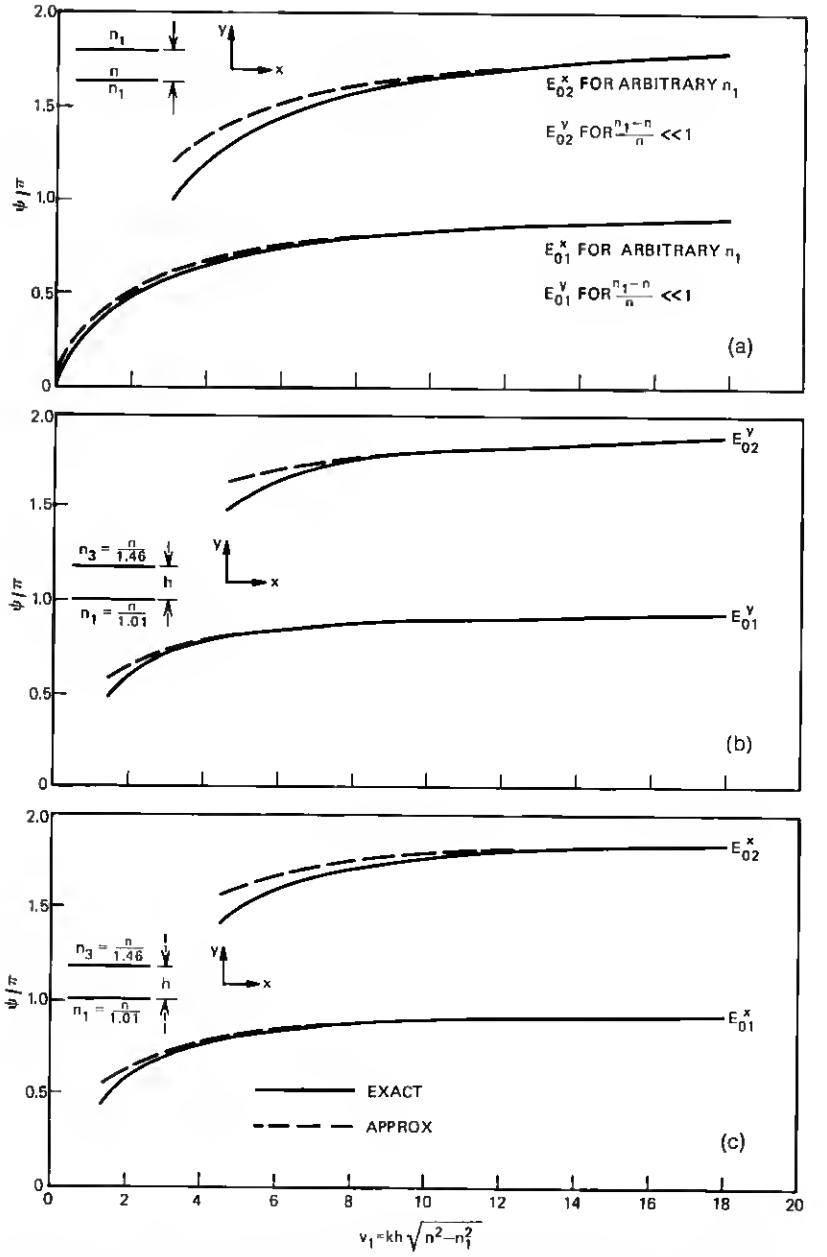

Fig. 13—Exact and approximate width of dielectric slabs. (a) Symmetric slab. (b) Asymmetric slab (polarization along y). (c) Asymmetric slab (polarization along x).

A geometrical interpretation of the equivalence of the slabs can be gained from the field intensity distrihutions shown in Fig. 12(c).

APPENDIX B

Solution of the slab-coupled guide

The exact solution of Maxwell's equations for the dielectric guide whose cross section is shown in Fig. 6(b) is very difficult because the boundaries are not analytical. However, a good quantitative insight can be gained if, as in Ref. 14, good guidance is assumed, that is, if most of the electromagnetic energy is contained within the guide. Then the field in the shaded areas, Fig. 6(b), can be ignored and the slah solution of Appendix A can be applied independently to each of the finite slabs of widths h, w, and t that make the guide. Thus, another dielectric guide, Fig. 6(c), is derived which is equivalent to that in Fig. 6(b) in the sense of having the same axial propagation constant k_z and the same field penetration in the slabs of thicknesses t and T. Unlike the original guide that has four dielcctrics, the equivalent one has a single dielectric of index n and is surrounded by a hypothetical material that forces the transverse field components (along x and y) to he negligihly small on the houndaries and confines the electromagnetic energy within the guide. The dimensions of this equivalent guide are related to the original one by the following expressions derived from (82),

$$H = h(1 + c_h), \tag{83}$$

$$W = w(1 + c_w), \tag{84}$$

and

$$T = t(1 + c_t), \tag{85}$$

where

$$c_w = 2\frac{K_w}{v_w}, \tag{86}$$

$$c_t = \frac{h}{t}\left(\frac{K_1}{v_1} + \frac{K_3}{v_3}\right), \tag{87}$$

$$K_w = \begin{cases} \dfrac{n_3^2}{n^2} & \text{for polarization along } x, \\ 1 & \text{for polarization along } y, \end{cases} \tag{88}$$

and

$$v_w = kw\sqrt{n^2 - n_3^2}, \tag{89}$$

and, because of thc choice of symhols, c_h coincides with (79).

To solve the boundary value problem of Fig. 6(c) we make further assumptions. One is that the slabs do not perturb the sinusoidal distribution of field in the core and vice versa. Another assumption, justified qualitatively in the text, is that only the fundamental mode of the slabs of thickness T contribute significantly to determine the propagation constants of the modes of the guide. Then, the characteristic equations of the core and slabs are

$$k^2n^2 = \left(\frac{\pi p}{W_e}\right)^2 + \left(\frac{\pi q}{H}\right)^2 + k_z^2 \tag{90}$$

$$k^2n^2 = -k_{xs}^2 + \left(\frac{\pi}{T}\right)^2 + k_z^2, \tag{91}$$

where p and q are the number of half periods along x and y, k_{xs} is the propagation constant in the x direction within the slabs, and W_e is the equivalent width of the core. W_e is somewhat different from W because of the field penetration from the core into the slabs.

To calculate W_e, we imagine the core divided by the dotted line in two regions, a and b. In region a the width is W. In region b the electrical width $\phi = k_xW$ is given by the slab equation[13]

$$\pi p = \phi + 2\tan^{-1}\frac{\phi}{k_{xs}W}. \tag{92}$$

With the value of k_{xs} deduced from (90) and (91) and considering that $W_e \cong W$, eq. (92) becomes

$$\pi p = \phi + 2\tan^{-1}\frac{\phi}{\sqrt{\left(\frac{\pi W}{T}\right)^2 - \left(\frac{\pi qW}{H}\right)^2 - (\pi p)^2}} \tag{93}$$

and its asymptotic solution is

$$\phi = \frac{\pi p}{1 + \frac{2T}{\pi W}\frac{1}{\sqrt{1 - \left(\frac{qT}{H}\right)^2}}}. \tag{94}$$

Following the procedure described in Appendix A, the equivalent width of the region b of the core results in

$$W_b = W\left[1 + \frac{2T}{\pi W}\frac{1}{\sqrt{1 - \left(\frac{qT}{H}\right)^2}}\right]. \tag{95}$$

We will assume the equivalent width of the core W_e to be a linearly weighted average of W and W_b. Therefore,

$$W_e = \frac{W(H - T) + W_b T}{H}$$

or

$$W_e = W(1 + c_q) , \tag{96}$$

in which

$$c_q = \frac{2}{\pi} \frac{T^2}{WH} \frac{1}{\sqrt{1 - \left(\frac{qT}{H}\right)^2}}. \tag{97}$$

From (90), (91), and (96), we derive the explicit values of the propagation constant of a mode and the penetration depth d_{pq} in the slab over which the field decays by $1/e$:

$$k_z = \sqrt{k^2 n^2 - \left[\frac{\pi p}{W(1 + c_q)}\right]^2 - \left(\frac{\pi q}{H}\right)^2} \tag{98}$$

and

$$k_{xs} = \frac{1}{d_{pq}} = \frac{\pi}{T} \sqrt{1 - \left[\frac{pT}{W(1 + c_q)}\right]^2 - \left(\frac{qT}{H}\right)^2}. \tag{99}$$

These results apply not only to the guides in Figs. 6(b) and 6(c) but also to the somewhat more general guide in Fig. 6(a) provided that (*i*) the curved edges depart only slightly from those in Fig. 6(b), (*ii*) no exponential decay of the field or, equivalently, no turning point is introduced by the wall deformations, and (*iii*) h and w are chosen to be

$$h = \sqrt{\frac{h_{\max}}{w_{\max}}}\, s \tag{100}$$

and

$$w = \sqrt{\frac{w_{\max}}{h_{\max}}}\, s, \tag{101}$$

where $h_{\max}$ and $w_{\max}$ are the maximum height and width of the core portion of index n in Fig. 6(a) and s, its cross-sectional area.

If exponential decay of the field were introduced by the wall deformation, the simple expression (98) developed for k_z would not be applicable.

The choice of h and w in (100) and (101) are derived from the WKBJ method[15] or from the almost ohvious demands:

$$hw = s$$

and

$$\frac{h}{w} = \frac{h_{\max}}{w_{\max}},$$

which mean that hoth portions of core with index n in Figs. 6(a) and 6(b) have equal surface and equal aspect ratio.

After so many approximations one wonders ahout the percentile errors in the final results (98) and (99). We can have some impression of the precision achieved hy checking (98) against the more exact results developed elsewhere[11] in order to dimension an optical fiber of circular cross section at cutoff for the second mode, assuming small difference of refractive indexes hetween core and cladding.

Calling a the radius of the fiher core, the pertinent values for (99) are

$$n_1 = n_2 = n_3,$$

$$t = 0,$$

$$h = w = \sqrt{\pi}a \qquad \text{from (100) and (101),}$$

$$c_h = c_w = \frac{2}{\sqrt{\pi}V} \qquad \text{from (79) and (86),}$$

$$W = H = \sqrt{\pi}a\left(1 + \frac{2}{\sqrt{\pi}V}\right) \qquad \text{from (83) and (84),}$$

$$c_q = 0 \qquad \text{from (97),}$$

and

$$d_{pq} = 0,$$

where

$$V = ka\sqrt{n^2 - n_1^2}. \tag{102}$$

Substituting the values of d_{pq}, c_q, H, and W in (99), one obtains for $p = 1$ and $q = 2$, or for $p = 2$ and $q = 1$,

$$V = 2.83,$$

while the exact result is 2.4. The error of 18 percent is small indeed considering that at cutoff the assumption of negligihle field outside of the guide is crudely violated.

REFERENCES

1. P. Kaiser, E. A. J. Marcatili, and S. E. Miller, "A New Optical Fiber," B.S.T.J., *52*, No. 2 (February 1973), pp. 265–269.
2. P. Kaiser and H. W. Astle, "Low-Loss Single-Material Fibers Made from Pure Fused Silica," to be published in B.S.T.J., *53*, No. 7 (September 1974).
3. J. E. Goell, "Rib Waveguide for Integrated Optical Circuits," J. Appl. Optics, *12*, No. 12 (December 1973), pp. 2797–2798.
4. H. Noda, H. Furuta, and A. Ihaya, "A Novel Optical Waveguide for Integrated Optics," IEEE/OSA (1973), Conference on Laser Engineering and Applications, Washington, May 30–June 1, 1973.
5. V. Ramaswamy, "Strip-Loaded Film Waveguide," B.S.T.J., this issue, pp. 697–704.
6. J. A. Arnaud, "Transverse Goupling in Fiber Optics—Part II: Coupling to Mode Sinks," B.S.T.J., this issue, pp. 675–696.
7. E. A. J. Marcatili, "Bends in Optical Dielectric Guides," B.S.T.J., *48*, No. 7 (September 1969), pp. 2103–2132.
8. E. A. J. Marcatili and S. E. Miller, "Improved Relations Describing Directional Control in Electromagnetic Wave Guidance," B.S.T.J., *48*, No. 7 (September 1969), pp. 2161–2188.
9. D. Gloge, "Dispersion in Weakly Guiding Fibers," J. Appl. Optics, *10*, No. 11 (November 1971), pp. 2442–2445.
10. S. E. Miller, E. A. J. Marcatili, and Tingye Li, "Research Toward Optical-Fiber Transmission Systems," Proc. IEEE, *61*, No. 12 (December 1973), pp. 1703–1751.
11. D. Gloge, "Weakly Guiding Fibers," J. Appl. Optics, *10*, No. 10 (October 1971), pp. 2252–2258.
12. D. Gloge, "Bending Loss in Multimode Fibers with Graded and Ungraded Core Index," J. Appl. Optics, *11*, No. 11 (November 1972), pp. 2506–2512.
13. P. K. Tien, R. J. Martin, and G. Smolinsky, "Formation of Light-Guiding Interconnections in an Integrated Optical Circuit by Composite Tapered Film Coupling," J. Appl. Optics, *12*, No. 8 (August 1973), pp. 1909–1917.
14. E. A. J. Marcatili, "Dielectric Rectangular Waveguide and Directional Goupler for Integrated Optics," B.S.T.J., *48*, No. 7 (September 1969), pp. 2071–2102.
15. P. M. Morse and H. Feshback, *Methods of Theoretical Physics*, New York: McGraw-Hill, 1953, pp. 1092–1099.